Research in Astron. Astrophys. **2012** Vol. **12** No. **10**, 1439–1450
http://www.raa-journal.org *http://www.iop.org/journals/raa*

Research in Astronomy and Astrophysics

The effect of Compton scattering on gamma-ray spectra of the 2005 January 20 flare *

Wei Chen and Wei-Qun Gan

Key Laboratory of Dark Matter and Space Astronomy, Purple Mountain Observatory, Chinese Academy of Sciences, Nanjing 210008, China; *w.chen@pmo.ac.cn*

Received 2012 March 23; accepted 2012 April 11

Abstract Gamma-ray spectroscopy provides a wealth of information about accelerated particles in solar flares, as well as the ambient medium with which these energetic particles interact. The neutron capture line (2.223 MeV), the strongest in the solar gamma-ray spectrum, forms in the deep atmosphere. The energy of these photons can be reduced via Compton scattering. With the fully relativistic GEANT4 toolkit, we have carried out Monte Carlo simulations of the transport of a neutron capture line in solar flares, and applied them to the flare that occurred on 2005 January 20 (X7.1/2B), one of the most powerful gamma-ray flares observed by *RHESSI* during the 23rd solar cycle. By comparing the fitting results of different models with and without Compton scattering of the neutron capture line, we find that when including the Compton scattering for the neutron capture line, the observed gamma-ray spectrum can be reproduced by a population of accelerated particles with a very hard spectrum ($s \leq 2.3$). The Compton effect of a 2.223 MeV line on the spectra is therefore proven to be significant, which influences the time evolution of the neutron capture line flux as well. The study also suggests that the mean vertical depth for neutron capture in hydrogen for this event is about 8 g cm^{-2}.

Key words: Sun: flares — Sun: gamma-rays — scattering: Compton scattering

1 INTRODUCTION

In solar flares, both ions and electrons are accelerated to high energies; the interactions between them and ambient nuclei produce gamma-rays, positrons, neutrons, and mesons (e.g., Chupp & Ryan 2009). Observations of gamma-ray emission give information about the nature of accelerated ions (see Kiener et al. 2006; Murphy et al. 2007) and about the physical properties of the ambient medium (Gan 2005). The first observation (Chupp et al. 1973) of gamma-ray spectra firmly established gamma-ray spectroscopy as a tool to study the active Sun (for example Ramaty et al. 1977; Murphy et al. 1987, 1991).

Gamma-ray line emissions in solar flares cover the energy band ranging from 0.4 to 8 MeV, including lines from de-excitation of nuclei, the 2.223 MeV line from neutron capture in hydrogen, and the 0.511 MeV line from positron-annihilation. Narrow de-excitation lines are produced by

* Supported by the National Natural Science Foundation of China.

accelerated protons, alpha particles (α), and ^{3}He interacting with ambient heavier nuclei, while broad lines result from interactions of accelerated C, N, O and other heavier nuclei with the ambient H and He. There are also many unresolved-lines that are blended with the gamma-ray continua.

Detailed theoretical calculations of a neutron capture line (Hua & Lingenfelter 1987; Hua et al. 2002) and gamma-ray lines (Ramaty et al. 1979; Ramaty & Murphy 1987) produced by interactions with accelerated ions were carried out before. Recently, Murphy et al. (2009) extended the gamma-ray line production model by incorporating the cross sections computed from the TALYS code (Koning & Duijvestijn 2006). This code was introduced into astrophysical calculations of nuclear reaction rates (Goriely et al. 2008; Spyrou et al. 2008) and radioactive nuclei yields in solar flares (Tatischeff et al. 2006).

The traditional method used for studying the spectrum of accelerated ions in solar flares is to estimate the fluence ratio of the $4-7$ MeV band to the neutron capture line (Murphy & Ramaty 1984; Hua & Lingenfelter 1987; Murphy et al. 2007). Gan (1998) developed a method which uses the time profiles of $4-7$ MeV and the neutron capture line to deduce the spectral evolution of accelerated ions. However, we should point out that the approach taken in our work is different. First and foremost, the whole solar de-excitation line spectrum was calculated under the assumption of various solar atmosphere abundances and accelerated ion compositions for a set of spectral indices of accelerated ions. Then by use of these template spectra, we fit the observed spectrum to determine the best parameters of the accelerated ion spectrum.

Compton scattering has been studied by several authors (Bai & Ramaty 1978; Kontar et al. 2006), who showed that this process can significantly modify the bremsstrahlung spectra. However, these initial studies focused on sub-MeV energies. Kotoku et al. (2007), on the other hand, studied the Compton scattering of gamma-rays produced by energetic electrons via the bremsstrahlung process.

In the present work, we focus on the propagation of high-energy photons experiencing a series of Compton scatterings. For this purpose, we employed a Monte Carlo simulation toolkit named GEANT4, which is widely used in experimental high-energy physics, to simulate the effect of Compton scattering on photons in a solar atmosphere. In Section 2 we present the calculations of the Compton-scattered continuum of the 2.223 MeV neutron capture line as a function of depth. In Section 3, we apply these results in *RHESSI* observations to see whether the Compton scattering on the 2.223 MeV line has a significant effect on the gamma-ray spectra. We also present time profiles of the neutron capture depth and the corrected neutron capture line flux. We summarize our conclusions in Section 4.

2 SIMULATION OF COMPTON SCATTERING

It is well known that nuclear de-excitation lines are produced in optically thin regions, where the attenuation in the transport process is negligible. However, the 2.223 MeV neutron capture line is mostly produced in the deeper chromosphere or even the photosphere (Hua & Lingenfelter 1987), and the Compton scattering can modify the resulting emission characteristics.

The GEometry ANd Tracking version 4 (GEANT4) Monte Carlo simulation toolkit (Agostinelli et al. 2003) is a platform for simulations of the passage of particles through matter. Developed at CERN by experimental high-energy physicists, GEANT4 has the following important features: firstly, it allows a very flexible construction of the "geometry" in which particles interact; secondly, it can "track" an individual particle while monitoring its physical quantities, such as the energy, momentum, position, and time lag; thirdly, it allows us to incorporate the desired interactions, in the present case, including multiple scattering and capture of neutrons, and Compton scattering of photons. The pair-production is neglected because at 2.223 MeV in hydrogen plasma, the total pair-production cross section is approximately three orders of magnitude smaller than the total Compton cross section. The photoelectric effect is also neglected because it is only dominant at lower energy (< 100 keV).

Using the GEANT4 toolkit, we simulated the effects of Compton scattering on isotropic 2.223 MeV photons passing through a spherical shell of the solar atmosphere with a series of depths, and recorded the escaping photons' energies to determine the expected spectra. Then we compared these results with observations to constrain the depth of neutron capture processes.

The dependence of the Compton effect on the depth of neutron capture photon production was examined by carrying out a series of simulations in which 2.223 MeV line photons were released at specific atmospheric depths with the ^{4}He/H ratio of 0.1.

Figure 1 shows the Compton scattered spectra of the 2.223 MeV line for different depths ranging from 1.0 to 50.0 g cm^{-2}. We can see that the Compton effect of the 2.223 MeV line decreases sharply with decreasing neutron capture depth. Moreover, the Compton-scattered continuum has a relatively flat spectrum at energies between the 2.223 MeV line and $\sim$1 MeV and becomes steep below $\sim$1 MeV. As a measure of the relative strength of the Compton scattered spectrum for various depths, we assume that the Compton-scattered continuum is a uniform spectrum which extends from 0 to 2.223 MeV. Also we consider the average number of photons per keV of the scattered component at the $1-2.22$ MeV band as that of the whole Compton-scattered continuum. Here we neglect the slope of the continuum below the 1 MeV band because positron-annihilation photons and bremsstrahlung photons tend to dominate the counting rates at these energies in flare spectra.

One can then define the *Compton Efficiency* as the ratio of the Compton-scattered continuum intensity to the intensity of the 2.223 MeV line. We have approximated these results by the expression

$$D = 14.53 \times CE + 0.62\,. \tag{1}$$

Here $CE = I_{\rm c}/I_{\rm l}$ is *Compton Efficiency*, $I_{\rm l}$ is the 2.223 MeV line intensity and $I_{\rm c}$ is the Compton-scattered continuum intensity. This equation can be used to estimate the depth of production of the neutron capture line. For flare analysis, it should be noted that D in Equation (1) is the line-of-sight depth in units of g cm^{-2}. Since the height and size of a flare is typically small when compared to the solar radius, the transformation of the line-of-sight depth to the vertical depth is just multiplied by a cosine of heliocentric angle. An accurate calculation must take into account the dependence of depth on the density of the solar atmosphere since it has a strong up/down asymmetry. However, the preliminary simulation shows that there is no significant difference among scattered spectra resulting from backscattering at different depths, except a small effect that lowers the energy of the scattered spectrum.

Vestrand (1990) developed a Monte Carlo code for photon transportation to simulate the neutron capture photons in a semi-infinite plane-parallel atmosphere. The calculation indicated that the relative strength of the Compton tail increased with the depth of photon production. Based on the advanced Monte Carlo simulation code, GEANT4, we obtained similar results. The relative strengths of the scattered continuum are quantitatively consistent with each other. By incorporating the depth and Compton efficiency into Equation (1), it is easier to determine the neutron capture depth.

3 APPLICATION AND DISCUSSION

To investigate the role of Compton scattering in the gamma-ray spectra, we study in detail the X7.1/2B event on 2005 January 20, which occurred in active region 10720 at coordinates N14 W61 (with a heliocentric angle of $\sim$65°). This flare was well observed by *RHESSI*. The light curves are displayed in Figure 2. The background subtraction was done with the same method as Smith et al. (2003), taking 15 orbits before and after the flare. The temporal evolution of the flare looks simple, with only one dominant peak in gamma-ray energy bands. The light curves in this period consist of three phases: rise, peak, and decay. We have chosen the time interval 06:43:10$-$07:00:10 UT as our period of interest, and divided this period into 16 intervals for later calculations.

RHESSI observations with a high spectral resolution in gamma-ray enable us to analyze its continuum and line profiles. A full count spectrum from 250 keV to 16 MeV (the upper limit of energy

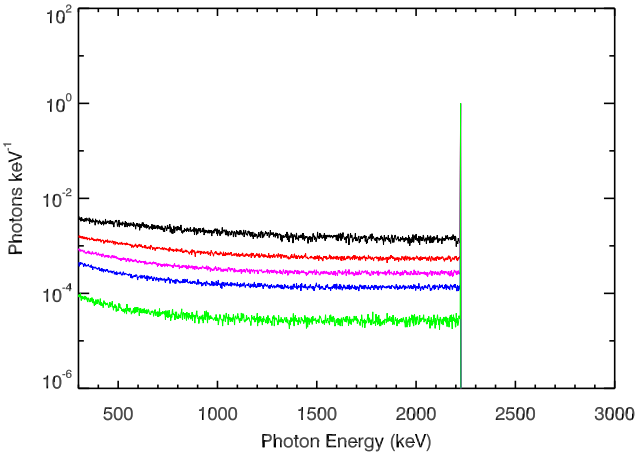

Fig. 1 Simulated Compton scattered spectra of 2.223 MeV photons for different vertical depths. The spectra have been normalized to the same intensity in the narrow 2.223 MeV line. Curves from top to bottom represent the results for total grammage of 50, 20, 10, 5 and 1.0 g cm^{-2}, respectively.

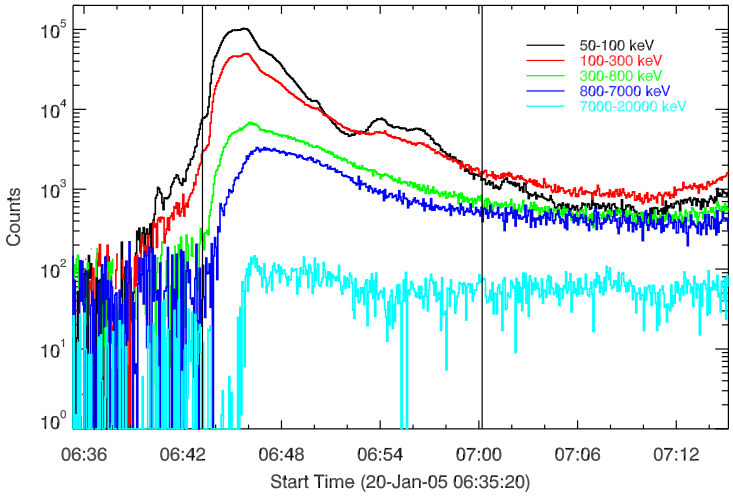

Fig. 2 Hard X-ray and gamma-ray light curves of the 2005 January 20 flare. The time interval of interest is between the two vertical lines (06:43:10−07:00:10 UT).

resolution with *RHESSI* data) can be fitted with a broken power-law which extends to 150 MeV, and two narrow Gaussian lines at 0.511 MeV and 2.223 MeV, as well as a template for gamma-ray spectra from accelerated ions. In our solar gamma-ray production model, the de-excitation line spectrum consists of narrow lines and continua. The narrow lines result from accelerated protons and α particles interacting with ambient heavy elements. Continua contain broad lines which are generated from accelerated heavy elements interacting with ambient H and He. Another unresolved-line continuum includes a series of weak lines, a compound continuum and pre-equilibrium continuum

(Chen & Gan 2012). The abundances of both accelerated particles and ambient elements are coronal (Reames 1995) except for the ambient ^{4}He/H ratio of 0.1 and the accelerated α/p ratio ranging from 0.0 to 1.0. All nuclear cross sections are calculated from the TALYS code, which has been verified by many authors. We have two assumptions in our calculation. First, we assume a downward-isotropic angular distribution of the accelerated ions. Share et al. (2003) showed that an isotropic distribution in the downward direction is better than a simple downward beam. Second, considering the effect of both angular distribution of ions and diversification of the nuclear reactions, we assume the isotropic gamma-ray emissions are in the excited nucler rest frame. In addition, we consider the effect of the flare location on the de-excitation line spectrum. Since the flare location is a known quantity of measurement, the de-excitation gamma-ray spectrum, therefore, depends on the spectral index of accelerated ions and the alpha to proton ratio (α/p). The continuous emission in the gamma-ray band is mainly from electron bremsstrahlung and π-decay. Because the shape of π-decay emission approximates a power-law distribution at energies below 16 MeV, we assume the broken power-law shape represents the continuous emission which blends the electron bremsstrahlung emission and π-decay emission.

The fitting was done by using the SPEX package (Schwartz et al. 2002) with different models. We did not consider the Compton scattering of the 2.223 MeV line in our first fitting model. The best-fitting result of the time interval 06:43:10−07:00:10 UT for this event is shown in Figure 3, in which the green curve represents the continuous emission component with a broken power-law shape, the yellow curve and the pink curve represent the positron-annihilation line (0.511 MeV) and the neutron capture line (2.223 MeV) respectively, and the cyan curve represents the total de-excitation lines which include the narrow lines and the continua. The sum of all these contributions is presented by the red curve.

The Compton scattering of the 2.223 MeV line was introduced in our second fitting model with an extra parameter of Compton-scattered continuum intensity.

Figure 4 shows the best-fit result. In this case, we can see a large contribution in the lower energy spectrum resulting from the Compton-scattered continuum of the 2.223 MeV line (purple curve).

Comparing both the best-fit results without and with Compton scattering in Figures 3 and 4 respectively, we note that the shape and intensity of the 0.511 MeV line has hardly changed in both cases. A similar situation is presented in the 2.223 MeV line. However, the accelerated ion spectrum of the latter fitting model is much flatter than that of the former. To determine the quality of fit, we use the statistic

$$\chi^2 = \Sigma[(c_i - m_i)/\sigma_i]^2 \tag{2}$$

as defined in Murphy et al. (1990), where c_i is the number of observed counts in channel i, m_i is the number of counts predicted by the model and σ_i is the uncertainty of the measurement in channel i. The minimum χ^2 values are 1291 and 1237 for these two models, respectively. We then plot a $\Delta\chi^2(\Delta\chi^2 = \chi^2 - \chi^2_{\rm min})$ contour map in the bottom right panel of Figures 3 and 4 which can be used to estimate the spectral index of ions and the alpha-to-proton ratio. By using a Monte Carlo simulation, the estimated $\Delta\chi^2$ values with 1σ uncertainty are 8.9 and 10 for these two cases, respectively. In addition, the residuals of fitting results are also improved with a smaller chi-square value in the second model, especially near 2 MeV. Both sets of evidence imply that the second model is better. Moreover, since the neutron capture photons are emitted at a vertical depth corresponding to a column density of about $10^{24} - 10^{25}$ H cm^{-2} (Hua & Lingenfelter 1987), the Compton effect of 2.223 MeV photons is naturally expected from a physical point of view. All results support that the second model is more reasonable in this event. The corresponding *Compton efficiency* is about 1.4 for the best fitting result of the second model. We thus infer from Equation (1) that the line-of-sight depth D is about 20 g cm^{-2}. Due to the off-diagonal response from the neutron capture line being significant for the *RHESSI*, we then estimated that the intensity of the Compton-scattered continuum has changed by about 20% for an uncertainty of instrumental response changing 10% in magnitude. So the vertical depth for neutron capture on hydrogen in this event is $8.5\pm0.3[\pm1.9]$ g cm^{-2}. Here

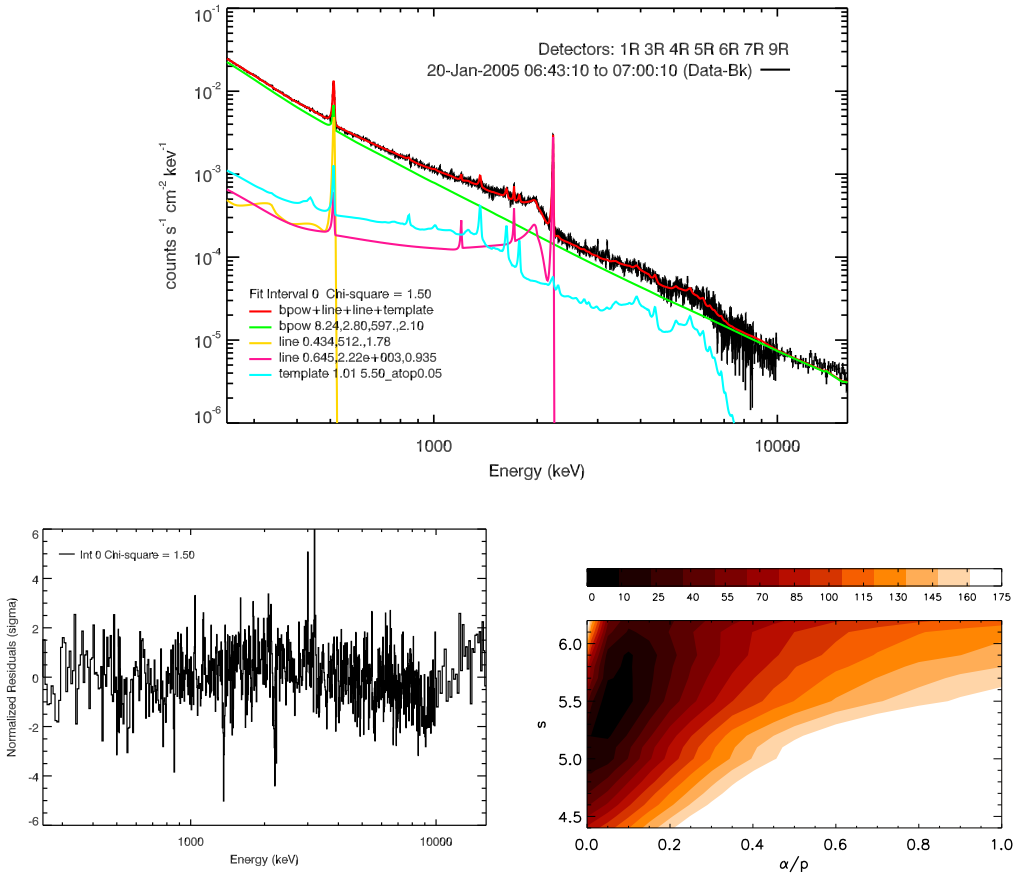

Fig. 3 *Top*: Fit to the background-subtracted spectrum of the time interval 06:43:10−07:00:10 UT for the 2005 January 20 flare. *Bottom left*: The residuals of this fit. *Bottom right*: $\Delta\chi^2$ contour for spectral index (s) and the alpha-to-proton ratio (α/p). The fit result shows that the accelerated ions have a spectral index of about $>$5.0 for an assumed power-law spectrum in this case.

the uncertainty of 0.3 is from fitting data and the uncertainty of 1.9 is from instrumental response. This depth is similar to that of the simulation for a hard ion spectrum (Hua & Lingenfelter 1987).

The results above can be understood as the following. Calculated de-excitation of gamma-ray spectra for various spectra of accelerated ions are shown in Figure 5.

The shape of the spectrum is very sensitive to the power-law index of accelerated ions. The narrow lines are more prominent for a soft spectrum ($s = 5.0$), while the continua dominate for a hard spectrum ($s = 2.0$). On the other hand, the unresolved components are much flatter relative to the broad components and do not present a bump at 1−2 MeV. A harder spectrum results in more interactions involving high-energy ions (protons and heavies), which tend to produce stronger unresolved components because their cross sections extend to higher ion energies than those for resolved lines. In addition, Figure 5 also shows that the unresolved components are stronger relative to the broad components for such a hard spectrum. For a soft spectrum, on the other hand, the broad components have become more important than unresolved components, particularly in the 1−2 MeV

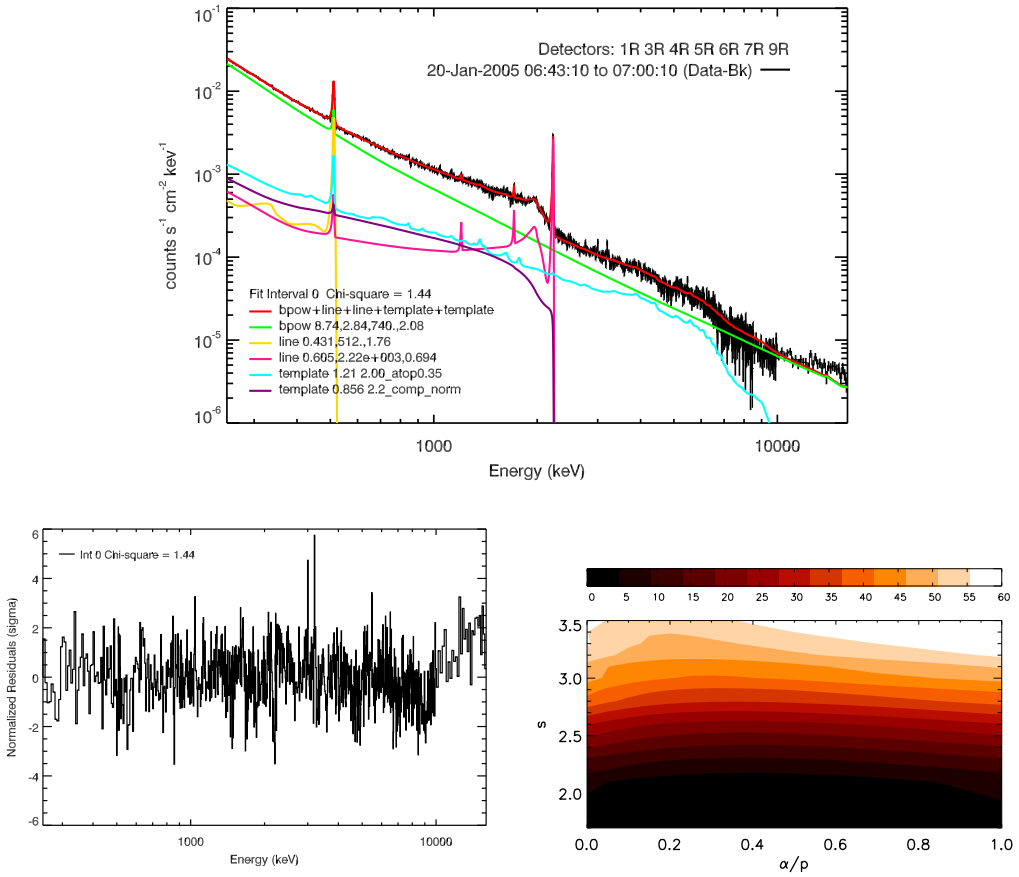

Fig. 4 Same as for Fig. 3, but adding the component of the Compton-scattered continuum of the neutron capture line (*purple curve*) in the fitting model. The fit result suggests the existence of a much harder spectrum, spectral index ≤ 2.3, in this case.

range. Therefore, the 1−2 MeV bump was noticeable in the soft spectrum. This shape is also similar to that for a Compton-scattered continuum of the 2.2 MeV line superposed on a photon spectrum for the hard ion spectrum. That is the reason why the ion spectrum becomes hard by introducing Compton scattering in the second model.

For a more quantitative analysis, we divided the above period into 16 successive time intervals and did a spectral fit with two models for each interval.

Figure 6 shows the evolution of the best-fit parameters of each model.

Both of the results seem to be reasonable in comparison with typical characteristics of gamma-ray events. Nuclear de-excitation line flux, neutron capture line flux, and positron-annihilation line flux all reach their peaks later than the bremsstrahlung flux. Furthermore, they all have a fast rise and gradual decay. The main difference between these two models is the evolution patterns of the spectral index of ions. The result of the second fitting model shows that the accelerated ion spectrum has an inclination to become hard with evolution. This characteristic was previously reported by Gan (2004) and Troitskaia et al. (2009).

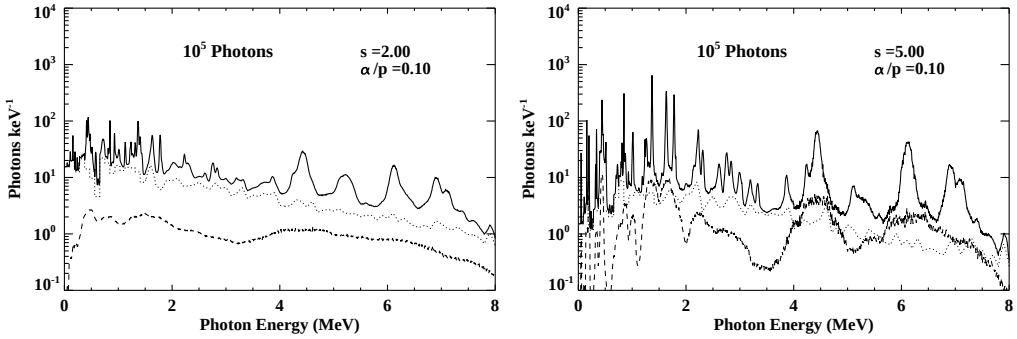

Fig. 5 Calculated de-excitation gamma-ray spectra versus the accelerated ion power-law index. The *left* panel shows the spectrum from accelerated ions with power-law index $s = 2.0$. The *right* panel shows the spectrum from accelerated ions with power-law index $s = 5.0$. The solid curves show total de-excitation gamma-ray spectra of the solar flare at a heliocentric angle of 60°, while the dashed curve and the dotted curve show the broad lines and the unresolved components, respectively.

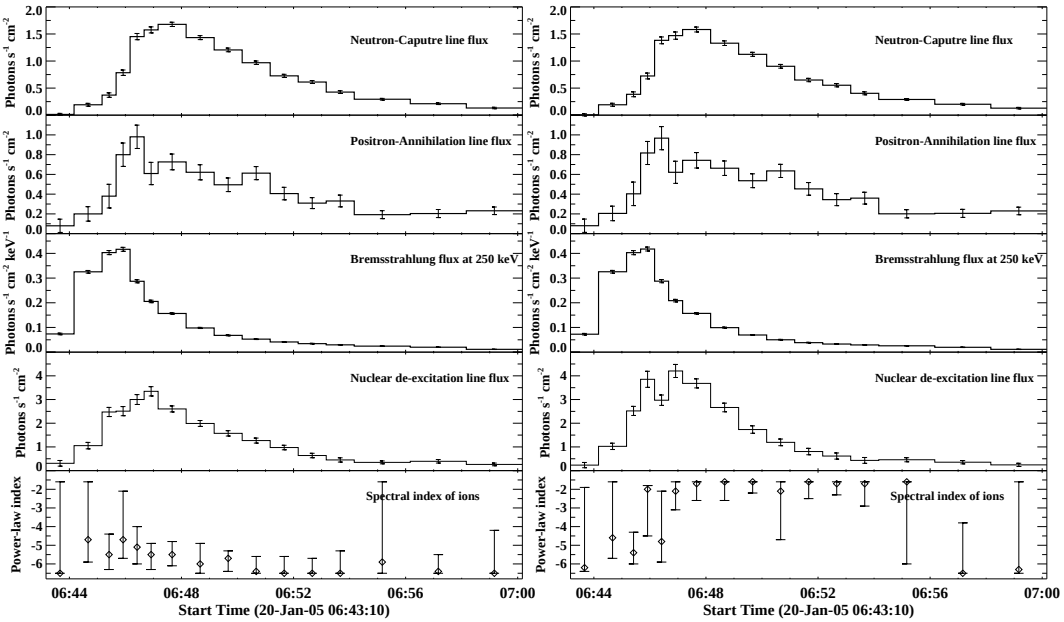

Fig. 6 Time evolution of the neutron capture line (2.223 MeV) flux, positron-annihilation line (0.511 MeV) flux, bremsstrahlung flux at 250 keV, nuclear de-excitation line flux, and power-law index of accelerated ion spectrum. The starting time of the figure is 06:43:10 UT. The *left* and *right* sides are best-fitting results without and with Compton scattering, respectively.

Besides the time profiles of line flux and spectral index, we also derive the time evolution of the Compton scattered component. In Figure 7 we show the time profiles of the neutron-capture line flux, the Compton-scattered continuum intensity, and the Compton efficiency for the flare. As can be seen, there is a strong correlation between neutron capture line flux and the Compton-scattered

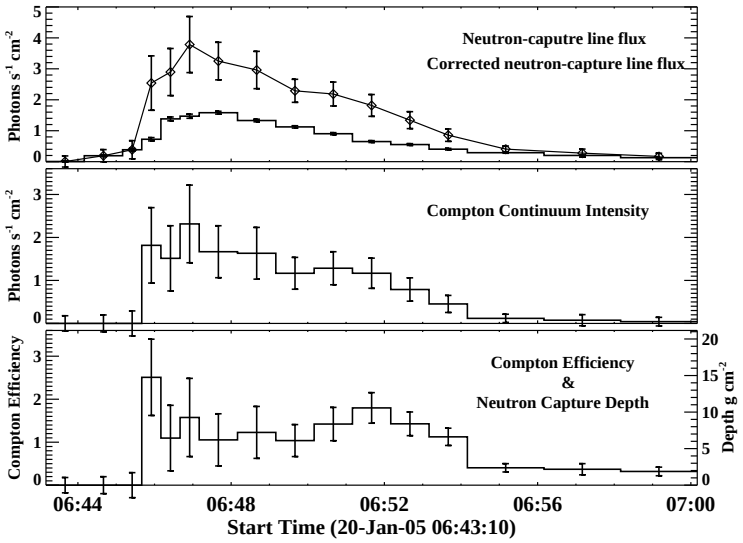

Fig. 7 Time profiles of the neutron capture line flux (*top panel*), the Compton-scattered continuum intensity (*middle panel*), and the Compton efficiency and the neutron capture depth (*bottom panel*) for the flare. The diamond symbol in the top panel represents the corrected neutron capture line flux.

continuum intensity of the 2.223 MeV line during some time period. However, the latter rises faster and lasts only several minutes. The Compton effect looks important, at least around the peak of the flare.

We can also see from Figure 7 that the Compton efficiency rises rapidly at the early phase, and then declines gradually. Combining the discussion with Equation (1), we can deduce how much column density is required for neutron capture on hydrogen in a solar flare. Most neutron capture photons are produced from the deeper atmosphere with the highest depth (about 15 g cm^{-2}) during the early phase. Subsequently, the photons produced from neutron capture are emitted from the higher atmosphere (lower depth) or formed within a more diffuse space relative to that at the early time.

The most effective neutrons for producing the 2.223 MeV line are those with energy below 50 MeV, which need to pass through a grammage of 10 g cm^{-2} for thermalization (Troitskaia et al. 2009). Consequently, our result of 15 g cm^{-2} implies the existence of higher energy neutrons at the early phase. In other words, it also indicates the existence of harder ion spectrum results in higher energy neutrons in this event. The corrected neutron capture flux by including the Compton-scattered continuum is also shown in the top panel by a diamond symbol. Since many neutron capture photons are converted to low-energy photons at the early phase, we can see that the peak of corrected neutron capture flux is about 1 minute earlier than that of the uncorrected flux. Therefore, the Compton scattering on the 2.223 MeV line is important for an accurate measurement of the neutron capture line flux.

The depth distribution of neutron capture on hydrogen depends primarily on neutron propagation. We use GEANT4 to find a decay time series. The monoenergy neutrons inject downward from the bottom of the chromosphere. The Sun is assumed to be a well-mixed plasma sphere of hydrogen and helium, having a series of shells stacked in the vertical direction with a density gradient. This assumption is basically reasonable, because the energy losses of neutrons are primarily determined by the column density of matter along its path. As a result, the histogram of neutron capture time reflects, to a certain extent, the depth distribution of neutron capture line production.

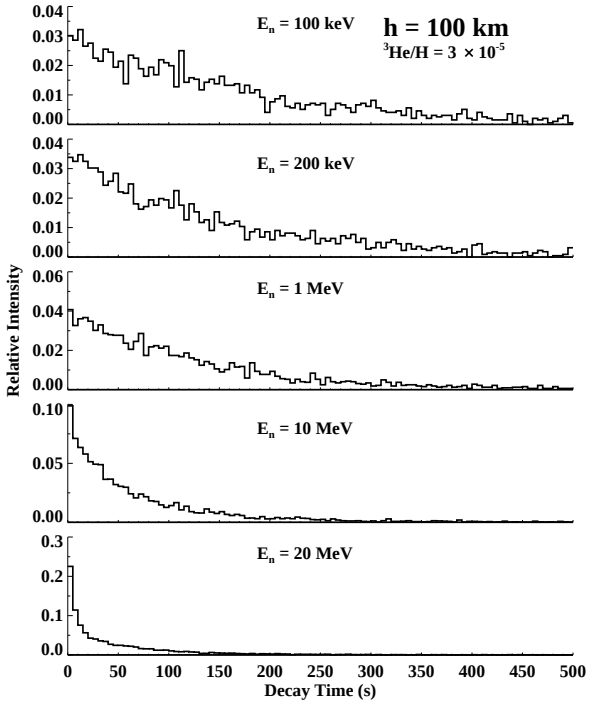

Fig. 8 Time history of neutron capture on hydrogen for different injected energy. The monoenergy neutrons are injected into the beam instantaneously at the same altitude. The different plots correspond to different initial neutron energies.

In the Monte Carlo simulation of neutron transport and capture, the most time-consuming part is the multiple scattering of the high-energy neutrons, because the scattering cross section is much larger than that of capture at this time. The capture cross section is inversely proportional to neutron velocities, so the capture process dominates low-energy neutrons rather than high-energy ones. The time history of various energy neutrons captured on hydrogen is shown in Figure 8. In this case, for a qualitative analysis, all neutrons are instantaneously released at the bottom of the chromosphere. One can see that the neutrons with higher energy are more easily captured at the early phase. Not confined by any magnetic fields, these high-energy neutrons can penetrate deeper into the atmosphere where they undergo more collisions, and can be easily thermalized and captured. For the same reason, the photons produced by neutron capture in this higher density region will encounter more scattering. With the flare continuing, however, many low energy neutrons were captured in the lower density atmosphere, since they did not have enough energy to be injected into the deeper atmosphere. Hence, the effect of Compton scattering on the 2.223 MeV line decreases after the rising phase.

4 SUMMARY

Because the region of thermalized neutron capture on hydrogen is mainly in the deeper atmosphere, the effect of Compton scattering on the neutron capture line cannot be ignored. In order to quantitatively estimate this effect, we have calculated the effect of Compton scattering on neutron capture photons from different depths. Specifically, we presented the equation in Section 2 that shows the strength of *Compton efficiency* depends on the vertical depth of the region where neutron capture occurs.

Observations from the hard X-ray/gamma-ray band would provide a strong constraint in understanding the mechanism of particle acceleration in flares. The present study is based on high resolution data from the *RHESSI* satellite. Our analysis is focused on gamma-ray spectra from the 2005 January 20 event. As expected, the derived neutron capture line, positron-annihilation line, and nuclear de-excitation lines are delayed with respect to the bremsstrahlung of 250 keV (Murphy et al. 2003) no matter whether Compton scattering on the neutron capture line is considered or not. However, when including Compton scattering, our analysis suggests the existence of a very hard ion spectrum with a power-law index ≤ 2.3 in this flare. On the other hand, the ratio of $\phi_{4-7}/\phi_{2.2}$, the fluence in the 4–7 MeV nuclear band to the fluence in the 2.2 MeV line, is measured to be about 0.40. Compared with the previous results (Murphy & Ramaty 1984), it also implies that a very hard ion spectrum existed in this flare. This derived hard spectrum of ions seems to be consistent with the subsequent solar energetic particle observations near $\sim$1 AU (Murphy et al. 2005; Krucker et al. 2005; Mewaldt et al. 2005), indicating that observed protons are possibly associated with the flare and not necessarily accelerated by the shock (Grechnev et al. 2008). Furthermore, by using a Compton-scattered continuum to correct the neutron capture line flux, we find that the time evolution has considerably changed, not only in terms of the intensity of the flux but also the time of the flux peak.

Through fitting the gamma-ray spectra of the 2005 January 20 flare, we have seen a sharp increase in the Compton efficiency at 06:45:40 UT, after about 2 minutes of gamma-ray onset, implying a substantial change in the spectrum of accelerated ions. With these measurements and calculations, we have evaluated the energy spectrum of accelerated protons and the depth of neutron capture of hydrogen for the Sun. The result shows that the neutron capture line averaged over the entire flare is emitted at a mean vertical depth of about 8 g cm^{-2}, which is similar to the simulation of Hua & Lingenfelter (1987). Furthermore, we find that the neutrons are captured by hydrogen at a vertical depth higher than 15 g cm^{-2} during the early phase of the flare. We conclude that Compton scattering has a significant effect on the propagation of 2.223 MeV photons, especially during the early phase of the flare.

The continuous model of our fitting above is assumed to be a broken power law, although in the real situation it might be or might depart from a broken power law. Different continuous models could lead to more or less different results, since the off-diagonal response to high-energy emission contributes in some degree to the low-energy count spectrum. However, the problem is that there is no observation at higher energy using the *RHESSI* detector. It is therefore hard at present to determine the exact shape of the continuum at higher energy. Future work can be done with different continuous models, such as the power law plus a power law times an exponential, so that one can compare the influence of different models on the results. Certainly, the final solution of the problem requires more higher energy observations.

Acknowledgements The authors are very grateful to the referee for helpful comments. Wei Chen thanks Gerald Share, Ronald Murphy, Jürgen Kiener, and David Smith for enlightening discussions. We wish also to acknowledge all the members of the *RHESSI* team for their excellent work. This work is supported by grants from the National Natural Science Foundation of China (Grant Nos. 10833007, 11078025 and 11173063) and the National Basic Research Program (973 program, Grant No. 2011CB811402).

References

Agostinelli, S., Allison, J., Geant4 Collaboration, et al. 2003, Nuclear Instruments and Methods in Physics Research A, 506, 250

Bai, T., & Ramaty, R. 1978, ApJ, 219, 705

Chen, W., & Gan, W.-Q. 2012, Chinese Astronomy and Astrophysics, 36, 49

Chupp, E. L., Forrest, D. J., Higbie, P. R., et al. 1973, Nature, 241, 333
Chupp, E. L., & Ryan, J. M. 2009, RAA (Research in Astronomy and Astrophysics), 9, 11
Gan, W. Q. 1998, ApJ, 496, 992
Gan, W. Q. 2004, Sol. Phys., 219, 279
Gan, W. Q. 2005, Advances in Space Research, 35, 1833
Goriely, S., Hilaire, S., & Koning, A. J. 2008, A&A, 487, 767
Grechnev, V. V., Kurt, V. G., Chertok, I. M., et al. 2008, Sol. Phys., 252, 149
Hua, X.-M., Kozlovsky, B., Lingenfelter, R. E., Ramaty, R., & Stupp, A. 2002, ApJS, 140, 563
Hua, X.-M., & Lingenfelter, R. E. 1987, Sol. Phys., 107, 351
Kiener, J., Gros, M., Tatischeff, V., & Weidenspointner, G. 2006, A&A, 445, 725
Koning, A. J., & Duijvestijn, M. C. 2006, Nuclear Instruments and Methods in Physics Research B, 248, 197
Kontar, E. P., MacKinnon, A. L., Schwartz, R. A., & Brown, J. C. 2006, A&A, 446, 1157
Kotoku, J., Makishima, K., Matsumoto, Y., et al. 2007, PASJ, 59, 1161
Krucker, S., Hurford, G. J., & Lin, R. P. 2005, AGU Fall Meeting Abstracts, # SH21A-01
Mewaldt, R. A., Cohen, C. M., Leske, R. A., et al. 2005, AGU Fall Meeting Abstracts, # SH23A-0320
Murphy, R. J., & Ramaty, R. 1984, Advances in Space Research, 4, 127
Murphy, R. J., Dermer, C. D., & Ramaty, R. 1987, ApJS, 63, 721
Murphy, R. J., Hua, X.-M., Kozlovsky, B., & Ramaty, R. 1990, ApJ, 351, 299
Murphy, R. J., Ramaty, R., Reames, D. V., & Kozlovsky, B. 1991, ApJ, 371, 793
Murphy, R. J., Share, G. H., Hua, X.-M., et al. 2003, ApJ, 595, L93
Murphy, R. J., Share, G. H., Smith, D. M., Shih, A. H., & Lin, R. L. 2005, AGU Fall Meeting Abstracts, # SH 23A-0311
Murphy, R. J., Kozlovsky, B., Share, G. H., Hua, X.-M., & Lingenfelter, R. E. 2007, ApJS, 168, 167
Murphy, R. J., Kozlovsky, B., Kiener, J., & Share, G. H. 2009, ApJS, 183, 142
Ramaty, R., Kozlovsky, B., & Suri, A. N. 1977, ApJ, 214, 617
Ramaty, R., Kozlovsky, B., & Lingenfelter, R. E. 1979, ApJS, 40, 487
Ramaty, R., & Murphy, R. J. 1987, Space Sci. Rev., 45, 213
Reames, D. V. 1995, Advances in Space Research, 15, 41
Schwartz, R. A., Csillaghy, A., Tolbert, A. K., et al. 2002, Sol. Phys., 210, 165
Share, G. H., Murphy, R. J., Smith, D. M., et al. 2003, ApJ, 595, L89
Smith, D. M., Share, G. H., Murphy, R. J., et al. 2003, ApJ, 595, L81
Spyrou, A., Lagoyannis, A., Demetriou, P., Harissopulos, S., & Becker, H.-W. 2008, Phys. Rev. C, 77, 065801
Tatischeff, V., Kozlovsky, B., Kiener, J., & Murphy, R. J. 2006, ApJS, 165, 606
Troitskaia, E. V., Arkhangelskaja, I. V., Miroshnichenko, L. I., & Arkhangelsky, A. I. 2009, Advances in Space Research, 43, 547
Vestrand, W. T. 1990, ApJ, 352, 353